# A Precision Estimation Method for Volumetric Changes


Devrim Akca
*Department of Civil Engineering Isik University*
Istanbul, Turkey
akca@isikun.edu.tr

Efstratios Stylianidis
*Sch. Spatial Planning and Development Aristotle University*
Thessaloniki, Greece
sstyl@auth.gr

Daniela Poli
*4DiXplorer AG*
Zurich, Switzerland
daniela@4dixplorer.com

Armin Gruen
*Chair of Information Architecture ETH Zurich*
Zurich, Switzerland
agruen@geod.baug.ethz.ch

Orhan Altan
*Department of Geomatics Engineering Istanbul Technical University* Istanbul, Turkey
oaltan@itu.edu.tr

Martin Hofer
*GeoVille Information Systems GmbH*
Innsbruck, Austria
hofer@geoville.com

Konstantinos Smagas
*GeoImaging Ltd*
Nicosia, Cyprus
kostas@geoimaging.com.cy

Victor Sanchez Martin
*Ingeniería Y Soluciones Informáticas S.L.*
Sevilla, Spain
vsanchez@isoin.es

Andreas Walli
*GeoVille Information Systems GmbH*
Innsbruck, Austria
walli@geoville.com

Elisa Jimeno
*Ingeniería Y Soluciones Informáticas S.L.*
Sevilla, Spain
elisa.jimeno@isoin.es

Alejandro Garcia
*Ingeniería Y Soluciones Informáticas S.L.*
Sevilla, Spain
agarcia@isoin.es



***Abstract*—Earth surface changes are often computed by comparing the sequences of digital elevation models (DEMs) so called the DEM of difference (DoD) method. We present an operational DEM generation, co-registration and DoD comparison software in which the surface changes are quantified in metric units of volume. A practical method, which is based on the law of error propagation, is developed to estimate the theoretical precisions of volumetric changes. The proposed pipeline can estimate the change of object volumes (in terms of loss and gain) together with their precision numbers. Change of the forest volume in a fire effected region in a test site is analyzed for the validation. The method can be used for various change detection applications related to forestry as well as other topics such as earthworks, geomorphology, mining, and urbanization.**



***Keywords—surface, volume, change, precision estimation, DEM of difference (DoD), co-registration, comparison***


## I. INTRODUCTION

Volume is the amount of 3D space enclosed by a topologically closed surface. It requires much more computational effort in terms of data collection, processing and dissemination aspects with respect to distance and area. It is an important quantity to measure many phenomena in the environment, such as static object modelling, dynamic flow [1], biomass [2], glacier [3], timber [4], forest [5-6] and landslide [7-10] measurements.

Although there are many studies to investigate object change either in height or planimetric dimensions, relatively less studies exist to analyse it in all three dimensions [11-12]. 3D methods give better insights to understand the spatial variability [3].

In geodetic and photogrammetric applications, the digital elevation models (DEMs) derived from data of terrestrial, aerial or satellite sensors are used to model pre- and post-state of object surfaces. Consequently, changes of object surface are analysed through the comparison of pre- and post-state DEMs. This procedure is known as DEM of difference (DoD), in which cell-by-cell computations are performed to calculate the total volume of change [13]. It is also called as sequential DEM differencing (SeqDEM) method [3]. Several applications are available, e.g. in glaciology [3][14], urbanisation [15], forestry [16] and morphology [17].

Volume values, if given solely, have limited worth unless the uncertainty budget is known [18]. Uncertainties of volumetric changes generated by the DoD methods have been investigated in several studies [19-22]. The variance and covariance of the height errors of the respective DEMs have been considered in [23-25].

We developed an operational processing pipeline, implemented as a software package so called FORSAT, to generate digital surface models (DSMs) through the very high resolution satellite (VHRS) imagery and to perform the DoD method to obtain volumetric changes [26-28]. The VHRS imagery allows stereo and triplet overlaps at sub-meter resolutions, and offers cheaper, faster and more agile remote sensing capacities than the alternative imaging platforms. FORSAT software can also process the photogrammetric and LiDAR DSMs. A theoretical precision estimation method is developed in order to define the uncertainty budget of each volume value. It is a straightforward derivation of the law of error propagation.


978-1-5386-9448-0/19/$31.00 ©2019 IEEE

In the next chapter, FORSAT software is presented with the focus of its algorithmic details. In the third chapter, the precision estimation method is introduced. In the fourth chapter, the loss of forest volume due to a wild fire is analysed by co-registering and comparing the pre- and post-fire DSMs. The conclusions are given in the fifth chapter.

## II. FORSAT APPROACH

The goal of the FORSAT (a **sat**ellite processing platform for high resolution **for**est assessment) software is to develop an independent, standalone and modular satellite-based monitoring system for two-dimensional forest canopy mapping and change detection purposes. Although it was specifically developed for forestry applications, it can be used for many terrain applications. The software (Fig. 1) has four main modules for

1) format conversion and image pre-processing,

2) geo-referencing,

3) DSM generation,

4) 3D co-registration, comparison and analysis.

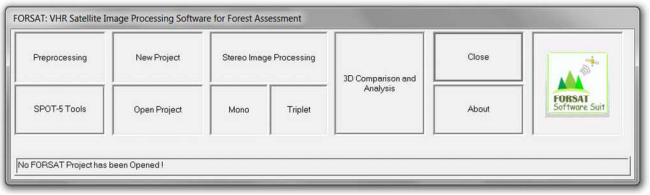


Fig. 1. FORSAT software and its user interface

The two main tasks are effectively combined under the entire system.

The first task is committed to the radiometric and geometric processing of the VHRS imagery and two- and three-dimensional surface information extraction. The sub-tasks are the image pre-processing, radiometric enhancement, tie-point and control-point measurement, image orientation and geo-referencing, quasi-epipolar image generation, dense image matching, DSM and ortho-image generation, and feature/vector measurement. Most of the optical VHRS imagery formats, such as Pleiades-1A/1B, WorldView-1/2, GeoEye-1, IKONOS, SPOT-5/6/7 are supported. The image formats from future missions are to be updated.

The second task is committed to three-dimensional point cloud and/or surface co-registration and comparison for change analysis. Not only the DSMs but also the digital terrain models (DTMs) can be imported and aligned by using a rigorous 3D surface matching method. Thereby, multi-temporal 3D models are used to calculate the 3D volume differences.

The FORSAT approach consists of a set of relevant algorithms all of which are the doctoral studies carried out at the group of photogrammetry of ETH Zurich. The technical details are explained in [29-31]. Afterwards, 4DiXplorer AG (www.4dixplorer.com), which is an ETH spin-off company located in Zurich, commercialized these algorithms. FORSAT is a customised software solution based on these algorithms and distributed by 4DiXplorer AG.

### A. Format Conversion and Image Pre-processing

Prior to the core algorithms, the conversion and enhancement operations are essential in order to make the input data ready. They comprise the analysis of the metadata files, extraction of the required image information (datum, orientation, intensity range, etc.), format conversion, creation of the internal image data files, and radiometric enhancement of the images in order to increase the reliability of point measurements.

The radiometric deficiencies are mostly out of control of the end-users. Their impact, which degrades the image quality, should be attenuated to the best of algorithmic abilities. The image pre-processing algorithms are employed so that such problems are reduced and the images are optimised for the subsequent measurement, feature extraction and matching steps. The common examples are the histogram equalisation, low-pass and high-pass filters, gamma correction and contrast enhancement, which are standard options in many of the image processing software packages. In this respect, the Wallis filter is a distinctive and powerful algorithm [32]. It applies a radiometric transformation such that the mean and standard deviation of the grey values of an image are shifted to user-defined target values. The FORSAT software uses the Wallis filter as the pre-processing method.

The image pyramids are used to represent an image in multi-resolution form. They are effective solutions to increase not only the speed but also the reliability of image matching computations meanwhile keeping the finest spatial resolution level. If a coarse-to-fine resolution hierarchy and an image pyramid are combined under a smart strategy, the matching results found at a coarse resolution are used to find denser matches at a finer resolution level. The computations are performed consecutively starting from the coarsest to the finest (original) levels of the image pyramid. The results of the coarser levels are the approximate information for the successor finer levels. FORSAT software generates the image pyramids starting from the original resolution images. In order to generated each pyramid level, a 7x7 pixel Gaussian kernel is multiplied and the resolution is reduced by factor 3. There are totally four levels including the base (original) level 0.

### B. Geo-referencing

The rational function model (RFM) is a widespread generalised (non-rigorous) orientation method based on the rational polynomials functions. The image pixel coordinates are expressed as the ratio of two polynomials, which are derived from the rigorous sensor model and the corresponding terrain information. The object coordinates, which are the normalized latitude, longitude and height values, stand as the multipliers to these rational polynomials coefficients (RPCs). The RFM does not reveal the sensor parameters, explicitly. The VHRS images are usually supplied with only the RPCs instead of rigorous sensor model parameters.

If a few numbers of control points are available, FORSAT software can improve the geo-referencing accuracy of the RFM through a kind of RPC block adjustment computation [33-35]. It can handle the stereo, triplet and block types of image acquisition configurations.

### C. Automated DSM Generation

FORSAT software uses an automatic DSM generation method which is based on the multiple primitive multi-image (MPIM) matching method [30][35][36]. It matches a dense pattern of features with an advanced matching strategy, exploiting all implicit and explicit knowledge, such as image acquisition network, sensor model, photogrammetric constraints (such as epipolar constraint) and image content. It

is an effective combination of feature-based and area-based image matching methods under the framework of parameter self-tuning, dense matching and coarse-to-fine hierarchical matching strategies [37-38].

Once the images and their associated pyramids are prepared in the pre-processing step, the area-based and the feature-based matching methods are run in parallel. Starting from the low resolution levels of the pyramids, the matching procedure progressively approaches eventually to the original resolution images. Any number of images can simultaneously be processed, since the procedures is based on the concept of multi-image matching, which is guided from the object space. The triangulated irregular network (TIN) is reconstructed from the matched features on each level of the pyramid using the Delaunay triangulation method, which in turn is used in the subsequent pyramid level for the approximations and adaptively computation of the matching parameters. Then, the least squares matching methods are used to achieve more precise matches for all the features and to identify the false matches. Finally, the DSM is resampled.

### *D. DSM Co-registration and Comparison*

In the DoD methods, a reference (template) DSM is interpolated in the DSM to be checked for quality evaluation, inspection and change detection purposes. This approach is suboptimal since:

- The errors in surface modelling may cause large height differences at surface discontinuities although the measurements are correct,
- if the template and the search DSMs have the reference frame differences, such as translations and rotations, then again large height differences may occur, especially at surface discontinuities although the heights are correct [36][38].

The height differences (one-dimensional along the Z-axes) may not truly represent the surface-to-surface distance in areas where the object surface is complex and undulated. Such drawbacks can be resolved by employing the approaches which use the Euclidean (3D) distance instead of the height difference [39-41].

FORSAT software uses a fully satisfying and general solution, which is the least squares 3D surface matching (LS3D) method [31][39][40][42]. It is a rigorous algorithm for the matching of overlapping 3D surfaces and/or point clouds. It estimates the transformation parameters of one or more fully 3D surfaces with respect to a template surface, using the generalised Gauss–Markov model, minimising the sum of the squares of the Euclidean distances between the surfaces. This formulation gives the opportunity to match arbitrarily oriented 3D surfaces, without using explicit tie points. Details of the procedure can be found in [43-44]. Diverse applications ranging from cultural heritage and object modelling to geomorphology are available [45-49]. The 3D co-registration and comparison module of the FORSAT software is a customised implementation of the LS3D method.

The procedure starts with matching of the pre- (template) and post-state (search) DSMs by use of the LS3D co-registration module of the FORSAT software. Once the DSM pair is co-registered and overlaid, the two surfaces form many shapes (3D manifolds) at intersection or separation regions. Each grid cell is analysed by comparing the template and search surface elements in it, and accordingly labelled as any of those three classes: decrease, no change and increase. As the grid cell dimensions and surface-to-surface distances are known, the area and volume values are computed by aggregating the information of all grid cells.

## III. PRECISION ESTIMATION FOR VOLUMETRIC CHANGE

The standard deviation (theoretical precision) of the volumetric change value is computed from the internal data following the law of error propagation. Therefore, it is a kind of a priori precision estimation method.

Assume that the volume $V$ of any polygon with a 3D change is to be computed as

$$V = a(h_1 + h_2 + \cdots + h_n)\ . \tag{1}$$

In short,

$$V = a \sum_{i=1}^{n} h_i\ , \tag{2}$$

where $a$ is the area of the unit grid cell of the template DSM, which is $2\times2 = 4$ m$^2$ in our test site, $h_i$ are the height differences between the template and search DSMs at every grid cell location within the polygon, $n$ is the number of grid cells coinciding in the change polygon.

The standard deviation $m_v$ of the volume $V$ is computed by applying the law of error propagation to Eq. (2).

$$m_v^2 = \left[\frac{\partial V}{\partial a}\right]^2 m_a^2 + \sum_{i=1}^{n} \left[\left[\frac{\partial V}{\partial h_i}\right]^2 m_{hi}^2\right] \tag{3}$$

The a priori precision of the area of the unit grid cell $m_a$ is supposed to be errorless, therefore $m_a = 0$.

$$m_v^2 = \left[\frac{\partial V}{\partial h_1}\right]^2 m_{h1}^2 + \left[\frac{\partial V}{\partial h_2}\right]^2 m_{h2}^2 + \cdots + \left[\frac{\partial V}{\partial h_n}\right]^2 m_{hn}^2 \tag{4}$$

The a priori precision of the height differences are assumed to be equal, that is,

$$m_{h1}^2 = m_{h2}^2 = \cdots = m_{hn}^2 = m_h^2\ . \tag{5}$$

The value of $m_h$ can be computed as the root mean square error (RMSE) of the co-registration of small surface patches of the DSMs over flat and unchanged areas. It corresponds to the uncertainty of surface match at the grid cell level.

Then, Eq. (4) becomes

$$m_v^2 = n\, a^2\, m_h^2\ , \tag{6}$$

$$m_v^2 = a\, A\, m_h^2\ , \tag{7}$$

$$m_v = \sqrt{a\, A}\, m_h\ , \tag{8}$$

where $A = n\, a$ is the area of the change polygon.

The volume and the associated theoretical precision (standard deviation) values in Fig. 10 are computed using Eq. (9).

$$V \pm m_v \tag{9}$$

## IV. Experimental Results

Cyprus has a typical Mediterranean climate, with long dry summers from May to October, and mild winters from December to February, which are separated by short autumn and spring seasons. This dry climate conditions trigger frequent forest fires, boosted through human interventions, which increase the risk for the ecosystem. The forest fire of Saittas, which was raged in 2007, was defined as the test site for the validation. The area of interest (AOI) delimited by a red frame in Fig. 2 covers an area of about 45 km² and includes the city of Pelentri in the Limassol district.

Fig. 2. The AOI is located in the centre of Cyprus

There was an Ikonos stereo pair dated from October 2001 available in the archive (Fig. 3), which was used for the generation of the pre-fire DSM. For the actual date, no VHRS image was available, so a new Pléiades stereo acquisition was ordered for the specific area. The Pléiades coverage was acquired in July 2014 (Fig. 4). In spite of the long period between the event and image acquisition, disastrous impact of the fire to the local vegetation is still visible.

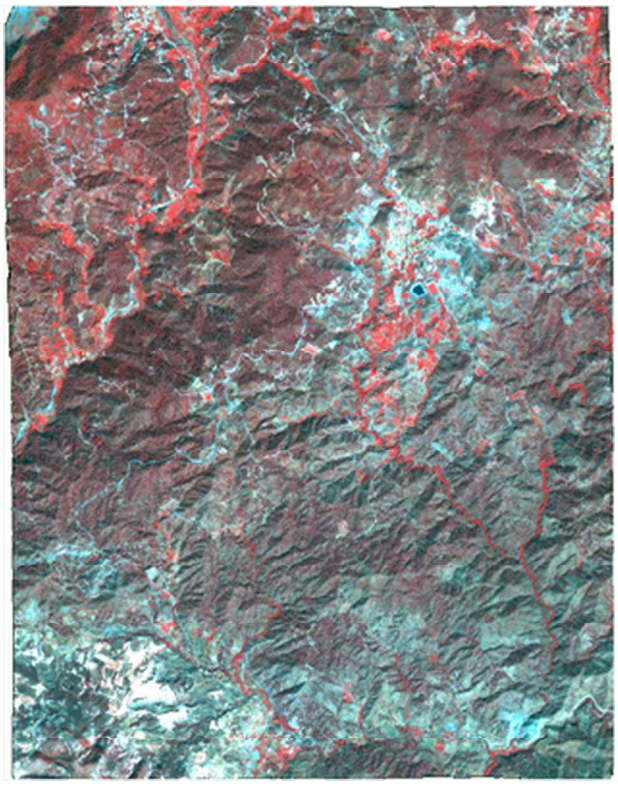

Fig. 3. Ikonos false color image composite of October 2001

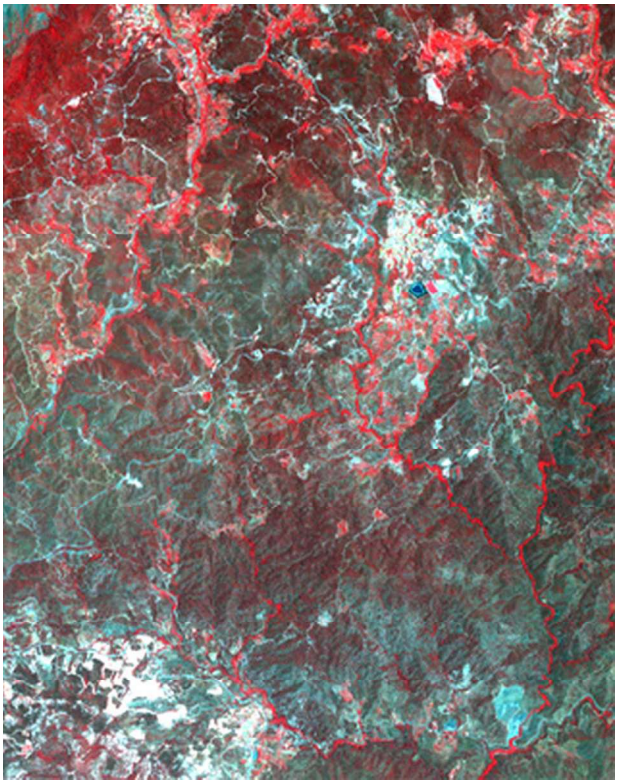

Fig. 4. Pléiades false color image composite of July 2014

Fig. 5. Pre-fire DSM gnerated from the images acquired in October 2001

Fig. 6. Post-fire DSM generated from the images acquired in July 2014

Based on the archived Ikonos stereo pair and the newly acquired Pléiades stereo pair, a historic (pre-fire) DSM (Fig. 5) and an actual (post-fire) DSM (Fig. 6) were generated using the FORSAT software. The both DSMs have the same spatial resolutions of 2.0 m.

On the basis of the generated DSMs, the change analysis was performed with the LS3D co-registration and comparison module of the FORSAT software (Fig. 7).

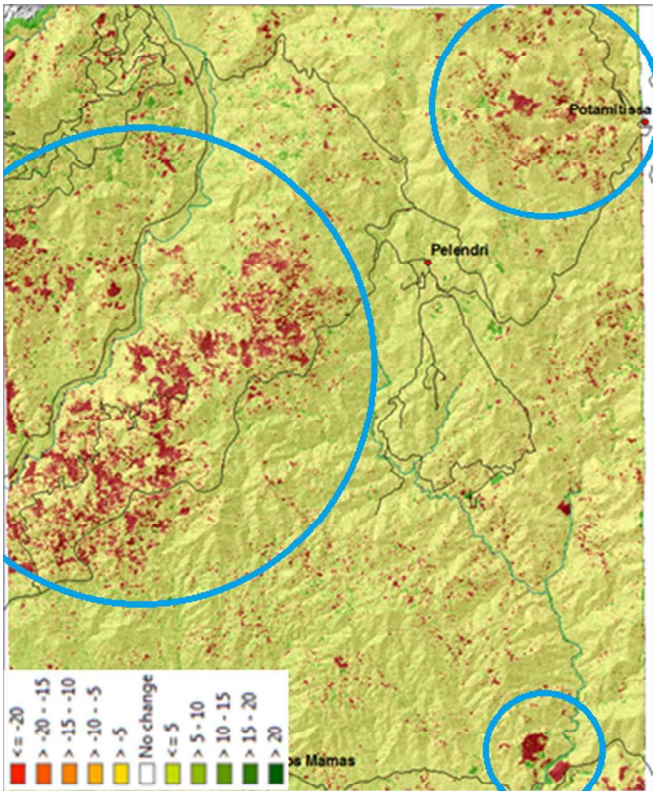


Fig. 7. Change map of the test site

The spatial deviations whose absolute values are greater than 3 m ($d > \|\pm 3\|$ m) between the historic and actual DSMs are labelled as a *change* (fire induced decrease or increase by vegetation growth). The used threshold value is the average a priori accuracy of the used DSMs according to our internal tests with the VHRS images. FORSAT software has an average DSM generation accuracy in the range of 2-to-3 times of the ground sampling distance (GSD) of the processed imagery.

The spatial deviations whose absolute values are less than 3m ($d \leq \|\pm 3\|$ m) are labelled as *no-change*.

As a consequence, three classes (*decrease-in-height*, *no-change* and *increase-in-height*) are identified in the change detection step.

The outliers (gross errors) due to image matching and modelling problems produce abrupt changes on the DSM surfaces. The spatial deviations whose absolute values are greater than 20 m ($d > \|\pm 20\|$ m) are considered as the outliers, excluded from the computation, and labelled as *no-data*. Despite the fact that they are excluded in the computations, they are kept in the visualizations.

The selection of the threshold values as ±3 m and ±20 m is specific to this application. They should be tuned depending on the data type and object of interest.

The outcome of the forest fire of Saittas is depicted in the change map (the largest blue circle in Fig. 7). Moreover, there are relatively smaller damaged areas in the north-east direction, near the Potamitissa village (the blue circle in the upper right part of Fig. 7). The change areas in the south-east direction of the AOI are the man-made changes (see the smallest circle in the lower right part of Fig. 7).

Fig. 8 shows the percentage of the vegetation type of the fire-affected coverage in the AOI. It is notable that the conifer forest (class 21) is the most affected vegetation type by the forest fire with nearly 70% of the area, followed by bushes and shrubs (class 23) with 9.5% and tree cultivations (class 27) with 9.2%.

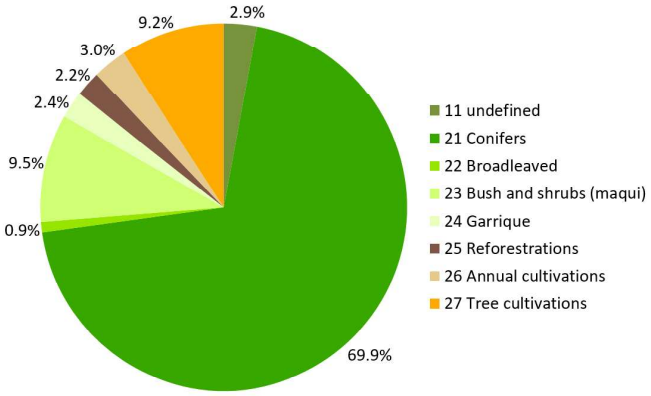


Fig. 8. Percentage of the vegetation type of the test site

Fig. 9 is a stacked column chart showing the internal change of each vegetation type according to the three change classes; *decrease*, *no-change* and *increase*. More than half (54.6%) of the broadleaved forest (class 22), 47.5% of conifer forest (class 21) and more than a third (36.0%) of the undefined forest (class 11) types were affected by decreasing the canopy height. Notice that the forest has not yet regenerated.

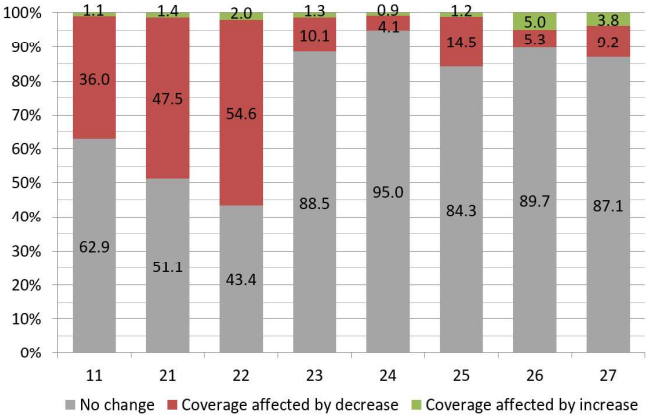


Fig. 9. Percentage of the internal change of each vegetation type

Fig. 10 shows the volumetric changes of fire-affected vegetation cover according to the DoD comparison of the DSMs of the year 2001 and 2014. It characterizes that there is the largest volume decrease (13,154,716 ±2,014 $m^3$) in conifer forest (class 21). Notwithstanding, this class has also the highest volume increase (365,892 ±341 $m^3$) in the site. Note that conifer forest covers almost 70% of the whole fire-affected area.

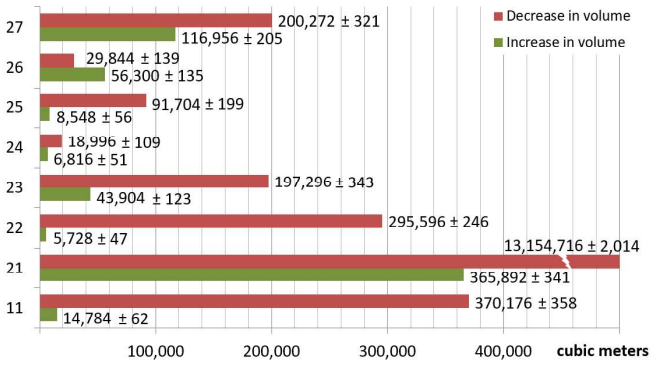


Fig. 10. Volumetric change ($m^3$) of each vegetation type

Bush and shrubs (class 23) and tree cultivations (class 27) are the land cover classes with a volume decrease of nearly 200,000 $m^3$. Moreover, the larger volumetric losses are exhibited in broadleaved (class 22) and undefined (class 11) forests. Apart from the conifer forest (class 21) only the tree cultivations (class 27) have a volume increase of more than 100,000 $m^3$. An interesting fact is that the annual cultivations (class 26) decreases the area, but increases the volume in net total.

The volume values and their standard deviations in Fig. 10 are computed according to the Eq. (9). In order to determine the $m_h$ value, the nine surface patches, each of which has a size of 25 x 25 points, are co-registered. Their locations are spatially well distributed in the extend of the AOI. The patches on the pre-fire DSM are set to the template, and the ones on the post-fire DSM are assigned as the search surface. They contain relatively flat terrain without any temporal change. Therefore, they are assumed to have only the random errors which show the quality of the fit of both DSMs. The average of the nine RMSE values coming from the nine co-registration computations is ±0.55 m which is taken as the $m_h$ value in Eq. (8). The coloured residuals on the template surface patches are given in Fig. 11.

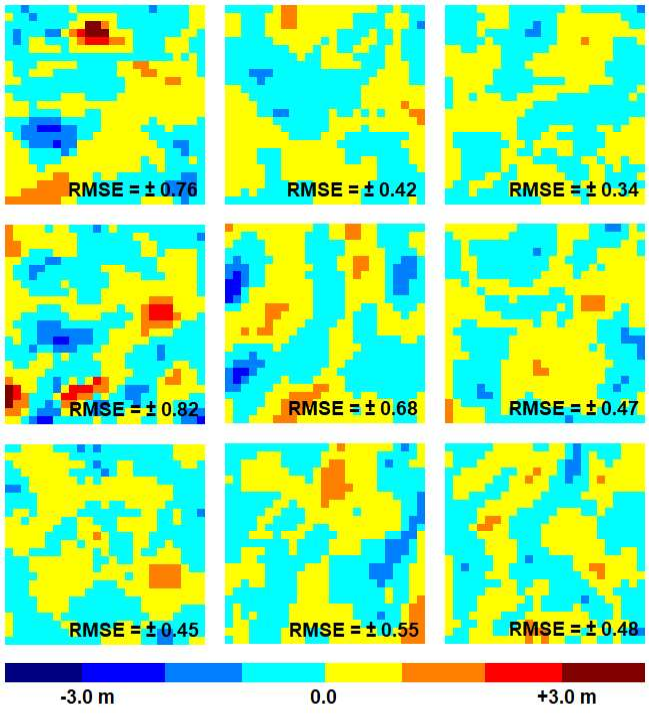


Fig. 11. Residuals of the nine co-registration computations

Value $m_h = \pm 0.55$ m does not represent the surface accuracy of the template and search DSMs. Rather, it shows the a priori precision of their fit at a minimal extend.

## V. Conclusions

A theoretical precision estimation method is proposed to assess the uncertainties of volumetric change values, which are generated by 3D comparison of pre- and post-event DSMs. It is based on the law of error propagation.

The developed software suite, so called FORSAT, generates the spatial information for rapid monitoring of environmental, natural and man-made changes. The basic input data is the VHRS imagery. The software consists of mutually linked modules which are pre-processing, geo-referencing, DSM generation, and 3D comparison and analysis.

The experimental study demonstrates the capability of FORSAT software for the change analysis of a forest burnt area. Pre-fire and post-fire DSMs were generated and compared. The volumetric gains and losses of the forest cover together with their standard deviation values helped us to gauge the severity and damage of the fire.

## References

[1] D. Schanz, F. Huhn, A. Schroeder, "Large-scale volumetric flow measurement of a thermal plume using Lagrangian Particle Tracking (Shake-The-Box)," in Particle Image Velocimetry, M. Raffel et al., Eds. Springer, 2018, pp. 606-610.

[2] S. Magnussen, T. Nord-Larsen, T. Riis-Nielsen "Lidar supported estimators of wood volume and aboveground biomass from the Danish national forest inventory (2012-2016)," Remote Sensing of Environment, vol. 211, pp. 146-153, 2018.

[3] R. Basantes-Serrano, A. Rabatel, C. Vincent, P. Sirguey, "An optimized method to calculate the geodetic mass balance of mountain glaciers," Journal of Glaciology, vol. 64, pp. 917-931, 2018.

[4] J. Rahlf, J. Breidenbach, S. Solberg, E. Naesset, R. Astrup, "Comparison of four types of 3D data for timber volume estimation," Remote Sensing of Environment, vol. 155, pp. 325-333, 2014.

[5] S. Puliti, S. Saarela, T. Gobakken, G. Stahl, E. Naesset, "Combining UAV and Sentinel-2 auxiliary data for forest growing stock volume estimation through hierarchical model-based inference," Remote Sensing of Environment, vol. 204, pp. 485-497, 2018.

[6] C. Xu, B. Manley, J. "Morgenroth,Evaluation of modelling approaches in predicting forest volume and stand age for small-scale plantations forests in New Zealand with RapidEye and LiDAR," Int. Journal of Applied Earth Observation and Geoinformation, vol. 73, pp. 386-396, 2018.

[7] D. Akca, A. Gruen, A. Askarinejad, S.M. Springman, "Photogrammetric monitoring of an artificially generated landslide,". The International Conference on GeoInformation For Disaster Management (Gi4DM'11), Antalya, Turkey, May 2011.

[8] D. Akca, "Photogrammetric monitoring of an artificially–generated shallow landslide," The Photogrammetric Record, vol. 28, pp. 178-195, 2013.

[9] A. Askarinejad, D. Akca, S.M. Springman, "Precursors of instability in a natural slope due to rainfall: a full-scale experiment," Landslides, vol. 15, pp. 1745-1759, 2018.

[10] C. Tang, H. Tanyas, C.J. van Westen, C. Tang, X. Fan, "Analysing post-earthquake mass movement volume dynamics with multi-source DEMs," Engineering Geology, vol. 248, pp. 89-101, 2019.

[11] R. Qin, J. Tian, P. Reinartz, "3D change detection – Approaches and applications," ISPRS Journal of Photogrammetry and Remote Sensing, vol. 122, pp. 41-56, 2016.

[12] T.H.G. Tran, C. Ressl, N. Pfeifer, "Integrated change detection and classification in urban areas based on airborne laser scanning point clouds," Sensors, vol. 18, pp. 448, 2018.

[13] S. Cucchiaro, M. Cavalli, D. Vericat, S. Crema, M. Llena, A. Beinat, L. Marchi, F. Cazorzi, "Monitoring topographic changes through 4D-

structure-from-motion photogrammetry: Application to a debris-flow channel," Environmental Earth Sciences, vol. 77, pp. 632, 2018.

[14] J. Podgorski, C. Kinnard, M. Petlicki, R. Urrutia, "Performance assessment of TanDEM-X DEM for mountain glacier elevetion change detection," Remote Sensing, vol. 11, pp. 187, 2019.

[15] D. Feurer, F. Vinatier, "Joining multi-epoch archival aerial images in a single SfM block allows 3-D change detection with almost exclusively image information," ISPRS Journal of Photogrammetry and Remote Sensing, vol. 146, pp. 495-506, 2018.

[16] K. Karila, X. Yu, M. Vastaranta, M. Karjalainen, E. Puttonen, J. Hyyppa, "TanDEM-X degital surface models in boreal forest above-ground biomass change detecetion," ISPRs Journal of Photogrammetry and Remote Sensing, vol. 148, pp. 174-183, 2019.

[17] M.A. Nunez-Andres, F. Buill, M. Hürlimann, C. Abanco, "Multi-temporal analysis of morphologic changes applying geomatic techniques. 70 years of torrential activity in the Rebaixader catchment (Central pyrenees)," Geomatics, Natural Hazards and Risk, vol. 10, pp. 314-335, 2018.

[18] X. Zhao, H. Alkhatib, B. Kargoll, I. Neumann, "Statistical evaluation of the influence of the u ncertainty budget on B-spline curve approximation," Journal of Applied Geodesy, vol. 11, pp. 215-230, 2017.

[19] C. Parente, M. Pepe, "Uncertainty in landslides volume estimation using DEMs generated by airborne laser scanner and photogrammetry data," International Archives of the Photogrammetry, Remote Sensing and Spatial Information Sciences, vol. 42, issue 3/W4, pp. 397-404, 2018.

[20] M. Avian, A. Kellerer-Pirklbauer, G.K. Lieb, "Geomorphic consequences of rapid deglaciation at Pasterze Glacier, Hohe Tauern Range, Austria, between 2010 and 2013 based on repeated terrestrial laser scanning data," Geomorphology, vol. 310, pp. 1-14, 2018.

[21] M. Scaioni, L. Barazzetti, M. Corti, J. Crippa, R.S. Azzoni, D. Fugazza, M. Cernuschi, G.A. Diolaiuti, "Integration of terrestrial and UAV photogrammetry for the assessment of collapse risk in Alpine Glaciers," The International Archives of the Photogrammetry, Remote Sensing and Spatial Information Sciences, vol. XLII-3, issue W4, pp. 445-452, 2018.

[22] C. Morino, S.J. Conway, M.R. Balme, J. Hillier, C. Jordan, P. Saemundsson, T. Argles, "Debris-flow release processes investigated through the analysis of multi-temporal LiDAR datasets in north-western Iceland," Earth Surface Processes and Landforms, 44, pp. 144-159, 2018.

[23] Y. Zhou, Z. Li, J. Li, R. Zhao, X. Ding, "Glacier mass balance in the Qinghai-Tibet Plateau and its surroundings from the mid-1970s to 2000 on Hexagon KH-9 and SRTM DEMs," Remote Sensing of Environment, vol. 210, pp. 96-112, 2018.

[24] Y. Zhou, J. Hu, Z. Li, J. Li, R. Zhao, X. Ding, " Quantifiying glacier mass change and its contribution to lake growths in central Kunlun during 2000-2015 from multi-source remote sensing data," Journal of Hydrology, vol. 570, pp. 38-50, 2019.

[25] M. Bagnardi, P.J. Gonzales, A. Hooper, "High-resolution digital elevation model from tri-stereo Pleiades-1 satellite imagery for lava flow volume estimates at Fogo Volcano," Geophysical Research Letters, vol. 43, pp. 6267-6275, 2016.

[26] D. Akca, E. Stylianidis, K. Smagas, M. Hofer, D. Poli, A. Gruen, V.S. Martin, O. Altan, A. Walli, E. Jimeno, A. Garcia, "Volumetric Forest Change Detection Through VHR Satellite Imagery," Int. Arch. Photogramm. Remote Sens. Spatial Inf. Sci., vol. XLI, issue B8, pp. 1213-1220, 2016.

[27] D. Akca, E. Stylianidis, D. Poli, A. Gruen, O. Altan, M. Hofer, K. Smagas, V.S. Martin, A. Walli, E. Jimeno, A. Garcia, "3-Dimensional pre- and post-fire comparison of forest areas," Int. Arch. Photogramm. Remote Sens. Spatial Inf. Sci., vol. XLII, issue 3/W4, pp. 9-16, 2018.

[28] D. Akca, E. Stylianidis, D. Poli, A. Gruen, O. Altan, M. Hofer, K. Smagas, V.S. Martin, A. Walli, E. Jimeno, A. Garcia, "Pre- and Post-Fire Comparison of Forest Areas in 3D," in Intelligent Systems for Crisis Management, O. Altan, M. Chandra, F. Sunar, T. Tanzi, Eds. Lecture Notes in Geoinformation and Cartography, Springer: Cham, 2019, pp. 265-294.

[29] D. Poli, Modelling of spaceborne linear array sensors, Ph.D. thesis, Mitteilungen Nr.85, Institute of Geodesy and Photogrammetry, ETH Zurich: Switzerland, 2005, pp. 1-217.

[30] L. Zhang, Automatic Digital Surface Model (DSM) Generation from Linear Array Images, Ph.D. thesis, Mitteilungen Nr.88, Institute of Geodesy and Photogrammetry, ETH Zurich: Switzerland, 2005, pp. 1-219.

[31] D. Akca, Least Squares 3D surface matching, Ph.D. thesis, Mitteilungen Nr.92, Institute of Geodesy and Photogrammetry, ETH Zurich: Switzerland, 2007, pp. 1-78.

[32] R, Wallis, "An approach to the space variant restoration and enhancement of images," Proc. of Symposium on Current Mathematical Problems in Image Science, Monterey, CA, USA, 1976.

[33] C. Fraser, E.P. Baltsavias, A. Gruen, "Processing of IKONOS imagery for sub-meter 3D positioning and building extraction," ISPRS Journal of Photogrammetry and Remote Sensing, vol. 56, pp. 177-194, 2002.

[34] J. Grodecki, G. Dial, "Block adjustment of high-resolution satellite images described by rational polynomials," Photogrammetric Engineering & Remote Sensing, vol. 69, 59-68, 2003.

[35] L. Zhang, A. Gruen, "Multi-image matching for DSM generation from IKONOS imagery," ISPRS Journal of Photogrammetry & Remote Sensing, vol. 60, pp. 195-211, 2006.

[36] L. Zhang, A. Gruen, "Automatic DSM generation from linear array imagery data," International Archives of Photogrammetry and Remote Sensing, vol. 35, issue B3, pp. 128-133, 2004.

[37] L. Zhang, S. Kocaman, D. Akca, W. Kornus, E. Baltsavias, "Test and performance evaluation of DMC images and new methods for their processing," ISPRS Commission I Symposium, Paris, July 2006.

[38] E. Baltsavias, S. Kocaman, D. Akca, K. Wolff, "Geometric and radiometric investigations of Cartosat-1 data," ISPRS Hannover Workshop on High Resolution Earth Imaging for Geospatial Information, Hannover, Germany, May 2007.

[39] A. Gruen, D. Akca, "Least squares 3D surface and curve matching," ISPRS Journal of Photogrammetry and Remote Sensing, vol. 59 pp. 151-174, 2005.

[40] A. Gruen, D. Akca, "Least squares 3D surface and curve matching," ISPRS Journal of Photogrammetry and Remote Sensing, vol. 59 pp. 151-174, 2005.

[41] D. Akca, M. Freeman, I. Sargent, A. Gruen, "Quality assessment of 3D building data," The Photogrammetric Record, vol. 25, pp. 339-355, 2010.

[42] D. Akca, "A new algorithm for 3D surface matching," International Archives of the Photogrammetry, Remote Sensing and Spatial Information Sciences, vol. XXXV, issue B7, pp. 960-965, 2004.

[43] D. Akca, A. Gruen, "Recent advances in least squares 3D surface matching," Optical 3-D Measurement Techniques VII, Vienna, Austria, vol. II, pp. 197-206, October 2005.

[44] D. Akca, A. Gruen, "Generalized Least Squares multiple 3D surface matching," International Archives of the Photogrammetry, Remote Sensing and Spatial Information Sciences, vol. 36, issue 3/W52, pp. 1-7, 2007.

[45] D. Akca, A. Gruen, Z. Alkis, N. Demir, B. Breuckmann, I. Erduyan, E. Nadir, "3D modeling of the Weary Herakles statue with a coded structured light system," International Archives of the Photogrammetry, Remote Sensing and Spatial Information Sciences, vol. XXXVI, issue 5, pp. 14-19, 2006.

[46] D. Akca, F. Remondino, D. Novàk, T. Hanusch, G. Schrotter, A. Gruen, " Performance evaluation of a coded structured light system for cultural heritage applications," Videometrics IX, Proc. of SPIE-IS&T Electronic Imaging, San Jose (California), USA, SPIE vol. 6491, pp. 64910V-1-12, January 2007.

[47] H.J. Seybold, P. Molnar, D. Akca, M. Doumi, M. Cavalcanti Tavares, T. Shinbrot, J.S. Andrade Jr., W. Kinzelbach, H.J. Herrmann, "Topography of inland deltas: Observations, modeling, and experiments," Geophysical Research Letters, vol. 37, pp. L08402, 2010.

[48] D. Akca, "3D modeling of cultural heritage objects with a structured light system," Mediterranean Archaeology and Archaeometry, vol. 12, pp. 139-152, 2012.

[49] D. Akca, H.J. Seybold, "Monitoring of a laboratory-scale inland-delta formation using a structured-light system," The Photogrammetric Record, vol. 31, pp. 121-142, 2016.